RSC Advances

PAPER

View Article Online
View Journal | View Issue

Cite this: *RSC Adv.*, 2015, **5**, 83781

Superior cycling stability and high rate capability of three-dimensional Zn/Cu foam electrodes for zinc-based alkaline batteries†

Zhao Yan,[ab] Erdong Wang,[a] Luhua Jiang[a] and Gongquan Sun*[a]

Three-dimensional (3D) Zn/Cu foam electrodes are fabricated by pulse electro-deposition of zinc on copper foam and investigated as negative electrode materials for zinc-based alkaline batteries. Scanning electron microscopy (SEM) images show that epitaxially layered zinc crystals distribute uniformly on the 3D copper foam-like skeleton. A peak power density of 286 mW cm^{-2} and utilization of 92% (754 mA h g^{-1} at 200 mA cm^{-2}) are obtained when the Zn/Cu foam electrodes are used in primary zinc/oxygen batteries and reveal high rate capability and material utilization of the 3D electrodes. To probe the rechargeability of the Zn/Cu foam electrodes, zinc/zinc quasi-symmetric cells are cycled under severe conditions, *i.e.*, a discharge–charge current density of as high as 250 mA cm^{-2}, 100% depth of discharge and without dendrite-suppressing additives that would otherwise suppress dendrite growth, yet the 3D Zn/Cu foam electrodes remain dendrite-free experienced 10 000 discharge–charge cycles. The specific capacity of the 3D Zn/Cu foam electrodes reaches up to 620 mA h g^{-1} after at least 9000 discharge–charge cycles in a prototype Zn/Ni battery, exhibiting the superior cycling stability of the 3D Zn/Cu foam electrodes.

Received 12th August 2015
Accepted 17th September 2015

DOI: 10.1039/c5ra16264e

www.rsc.org/advances

Introduction

Recently, with the fast increasing requirement for clean energy and especially environmental protection, economical and efficient energy storage/conversion devices particularly powering electric vehicles (EVs)[1,2] and electric grid energy storage (EGES),[3,4] have attracted much attention. Zinc, due to its rich reserves, non-toxicity, electrochemical stability in aqueous solution, and relatively high specific capacity, has been widely accepted as a desirable fuel in metal-based primary and secondary batteries,[5,6] such as zinc/air, zinc/nickel (Zn/Ni) batteries. As secondary batteries, zinc-based batteries are expected to possess properties including high energy density, competitive power density and good cycling stability. However, the traditional zinc electrode based on zinc powder suffers from insufficient conductivity, shape change and dendrite formation, and thus far away to satisfy the practical requirements, which hampers seriously the commercialization of zinc-based secondary batteries towards EV and EGES applications.[7]

Over the past years, extensive efforts have been made to improve the performance of zinc powder-based electrodes, by means of enhancing the electrical conductivity and/or suppressing the formation of dendrite. To improve the electrical conductivity, a conventional strategy is adding carbon black to zinc paste to strengthen the electrical connection between the active materials. By such a way, the maximum power density of a zinc/air battery was improved by 17.6% compared to the traditional electrode.[8] Zhang *et al.*[9] developed a zinc/air battery fabricated by fibrous zinc electrodes, which balanced the porosity and the electrical conductivity, in which the zinc utilization was as high as 86% at the discharge rate of 100 mA cm^{-2}. By adding conductive and porous magneli phase Ti_4O_7 to zinc electrode, the conductivity of the zinc electrode was improved and the dendrite was suppressed due to soluble zincate species being hold in porous surface structures. This Ti_4O_7 contained zinc electrode ran 320 discharge–charge cycles before its capacity fell below 90% of the initial capacity.[10]

Recent progress on self-supporting three-dimensional (3D) porous zinc electrode endows zinc-based secondary batteries excellent electrical conductivity and unobstructed mass transport. Parker *et al.*[11,12] designed 3D and fully metallic zinc sponges which remained dendrite-free after 45 discharge–charge cycles at 24 mA cm^{-2} benefiting from the interparticle conductivity of the monolithic 3D-wired zinc sponge electrode. However, the depth of discharge (DOD) of such a zinc self-supporting electrode is only 23%, which is unable to undertake a deep DOD, otherwise the 3D structure would collapse. To resolve the collapse of zinc electrode, Cheng *et al.*[13] proposed to deposit zinc on nickel foams, as a result, the power density and cycling stability of a single flow Zn/Ni battery were improved and a high coulombic efficiency of 97.3% and energy efficiency

[a]*Division of Fuel Cell & Battery, Dalian National Laboratory for Clean Energy, Dalian Institute of Chemical Physics, Chinese Academy of Sciences, Dalian 116023, China. E-mail: gqsun@dicp.ac.cn; Tel: +86-411-84379063*

[b]*University of Chinese Academy of Sciences, Beijing 100039, China*

† Electronic supplementary information (ESI) available: Supplementary data and schematic diagrams of test cells. See DOI: 10.1039/c5ra16264e

of 80.1% at 80 mA cm^{-2} over 200 cycles were obtained. However, the low hydrogen evolution overpotential of nickel foam leads to the formation of galvanic cell between zinc and nickel, which promotes the corrosion of zinc.

Till now, although great efforts have been made to improve the performance of zinc-based batteries, it is still full of challenges to develop a zinc electrode that meets both high metal utilization and good rate capacity together with excellent rechargeability. In this work, we fabricated a novel 3D electrode for zinc-based alkaline batteries by pulse electro-deposition of zinc on surface of 3D porous copper foam (Zn/Cu foam) at high current density, which ensured a uniform distribution of zinc on porous substrate. Taking advantage of the great merits of such an electrode, *i.e.*, (i) the large hydrogen evolution overpotential on copper substrate suppressing the self-corrosion of zinc efficiently; (ii) the stable copper framework throughout the discharge–charge period avoiding electrode collapse; (iii) the interconnected metal skeleton and macro-pores providing fast electron and mass transport; (iv) the porous structure providing a larger electrochemically active surface area for uniform distribution of active materials, the Zn/Cu foam electrode displayed a superior cycling stability (dendrite-free and potential-stable over 10 000 cycles) and high rate capability (92% capacity retention at 200 mA cm^{-2}) in zinc-based alkaline batteries.

Experimental

Materials

The copper foam (78.3 mg cm^{-2}, thickness: 2 mm, Dessco Electron, Kunshan), nickel foam (32 mg cm^{-2}, thickness: 1.7 mm, Tianyu Technology, Heze) and zinc plate (≥99.9%, Sinopharm Chemical Reagent, Shanghai) were cut into small pieces with the size of 2.5 × 2.5 cm^2 and washed with ethanol. After dried in ambient air, these materials were sealed with polyester to confine the effective area to 2.54 cm^2. Commercial air cathodes (J&N Energies, Tianjin) and sintered nickel electrodes (Highstar Battery, Jiangsu) were cut into squares with adequate size in order to fit with the zinc negative electrode. All other chemicals used in this study were of analytical grade and used as received without further purification.

Preparation of zinc electrodes

Copper foam was immerged in alkaline electrolyte containing 8.0 mol L^{-1} KOH and 0.5 mol L^{-1} ZnO between two zinc plates which served as counter electrodes in the electro-deposition process. A pulse current (current density: 1 A cm^{-2}, frequency: 250 Hz, duty ratio: 0.25) was applied to the electrodes and stopped after the calculated time to obtain the Zn/Cu foam electrodes.

To prepare zinc paste electrodes, 0.6 wt% sodium polyacrylate (QP-3, Huanyu chemical, Shenzhen), 0.6 wt% Carbopol® 941 polymer (Huanyu chemical, Shenzhen) and 98.8 wt% zinc powder (Ng-3305-1, Changgui metal powder, Zhejiang) were mixed with deionized water to form uniform paste and dried in oven at 40 °C for 12 h. After that, the electrode was prepared by pressing two zinc pastes and a copper mesh current collector at 1500 psi for 1 min in a stainless steel mold.

Electrochemical characterization

Cyclic voltammetries were carried out with a potentiostat (SI 1287A electrochemical interface, Solartron Analytical) in a traditional three-electrode cell, in which platinum plate was used as the counter electrode and Hg/HgO as the reference electrode in 7 mol L^{-1} KOH electrolyte. In this paper, all potentials were referred to the Hg/HgO electrode.

The primary zinc/oxygen battery was assembled with the Zn/Cu foam anode and the commercial air cathode (area: 2.54 cm^2) with the distance of 5 mm. An electronic load (ITECH Electronics, Nanjing) interfaced to a computer was employed to control the condition of discharging and record the voltage–current curves and constant current discharging curves. During the discharging process, the cathode of the zinc/oxygen battery was fed by oxygen at a flow rate of 50 sccm under atmospheric pressure.

The discharge–charge cycling performance was tested in a zinc/zinc quasi-symmetric cell and a prototype secondary Zn/Ni battery in alkaline electrolyte containing 8 mol L^{-1} KOH and 0.5 mol L^{-1} ZnO using a battery testing system (Neware Electronics, Shenzhen). Zn/Cu foam electrodes were placed between two zinc plates in the quasi-symmetric cell (Fig. S1†) test or two commercial sintered nickel electrodes in the prototype secondary Zn/Ni battery (Fig. S2†), respectively, with the distance for both electrodes of 30 mm. The area of zinc plate and commercial sintered nickel electrode were larger than working electrode to reduce the current density of counter electrode and mitigate the influence of their polarization to cell voltage.

The charge process was set stop at a fixed capacity, and the discharge process was set stop at 0.15 V offset *versus* onset discharge voltage for the zinc/zinc quasi-symmetric cell test or at the cut-off voltage of 1.0 V for the prototype secondary Zn/Ni battery to ensure complete discharging of zinc and reduce the accumulation of active materials on copper foam substrate which was found in our early studies, while the capacity for each discharge process was still calculated at 1.2 V to be comparable with other researches.[14–18] The discharge–charge process of the prototype secondary Zn/Ni battery was stopped at intervals for electrochemical impedance spectroscopy (EIS) analysis by using SI 1287A electrochemical interface and SI 1260 impedance/gain-phase analyzer (Solartron Analytical) with AC amplitude of 5 mV *versus* open circuit voltage and frequency range from 100 kHz to 0.1 Hz.

Physical characterization of Zn/Cu foam electrodes

The morphology of Zn/Cu foam electrodes after different discharge–charge cycles with fully charged state was examined by JSM-7800F scanning electron microscope. X-ray diffraction (XRD) patterns of the as-prepared Zn/Cu foam electrodes were conducted on X'pert Pro (PANalytical) diffractometer (60 kV, 55 mA) using Cu Kα radiation at a scanning rate of 5° min^{-1}.

Results and discussion

Screening metal substrate materials

To be an excellent substrate, the metal must be stable in alkaline electrolyte and the broad potential window (*ca.* −1 V to −2 V *vs.* Hg/HgO) during zinc dissolution/precipitation in the discharge–charge process and possesses large hydrogen evolution overpotential to reduce the self-corrosion of zinc. Fig. 1 illustrates the Tafel curves of different substrates in N_2 saturated 7 mol L^{-1} KOH solution. The corrosion potentials of copper foam, nickel foam and Zn/Zn plate (prepared by electrodepositing zinc onto zinc plate) are −0.485 V, −0.083 V and −1.465 V, respectively, which means both the copper foam and nickel foam are stable at the broad potential range during zinc dissolution/precipitation process. Fig. 2 shows the linear sweep voltammograms of different metal substrates in N_2 saturated 7 mol L^{-1} KOH solution. An obviously large hydrogen evolution overpotential and small hydrogen evolution current density at −1.465 V were obtained on copper foam. This indicates that zinc supported on copper foam may suffer less self-corrosion in alkaline electrolyte. Capacity retention curves in Fig. 3 show that the capacity of the as-prepared Zn/Ni foam electrode remains only 91.4% of theoretical capacity due to the severe hydrogen evolution reducing the current efficiency of zinc electrodeposition. After storage in 7 mol L^{-1} KOH solution for two days, capacity of Zn/Ni foam electrode drops to only 5% of the theoretical capacity, in contrast, Zn/Cu foam electrode remains 59% after ten days storage. These results reveal that copper foam is more suitable for zinc electrode support than nickel foam which was used as current collector in Zn/Ni batteries.[13–15,19]

Characterization of the Zn/Cu foam electrodes

Zinc electroplating is a mature technology which has been used for several decades in metal surface treatment. However, to prepare an excellent zinc electrode using this technology, rough and uniform zinc coating structure, instead of a compact protective film, is preferred in order to obtain large electrochemically active surface area and high loading of active materials. To achieve this aim, in our experiment, higher deposition current density[13] was adopted to obtain rugged surface in zinc electrode preparation compared with the traditional zinc electroplating. Moreover, pulse current and vigorous stirring were also carried out to prepare a uniform Zn/Cu foam electrode (Fig. S3–S5†). SEM images (Fig. 4) of copper foam substrate and Zn/Cu foam electrodes demonstrate that zinc crystals with epitaxially layered structure distribute uniformly on the 3D copper foam skeleton. X-ray diffraction patterns (Fig. S6†) reveal that metallic copper and zinc exist in Zn/Cu foam electrode. Although the particle size of zinc increases obviously with the increase of zinc loading (related to the electrode capacity), material distribution still remains unchangeable, which proves that the expected electrodes are prepared successfully by the above methods.

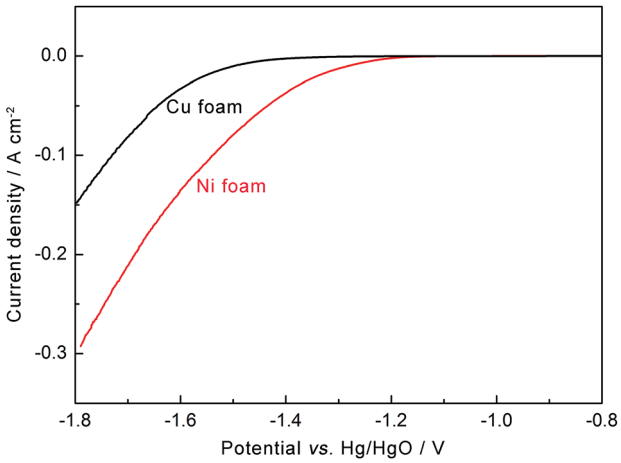

Fig. 2 Linear sweep voltammograms of different metal substrates (electrolyte: N_2 saturated 7 mol L^{-1} KOH, scan rate: 5 mV s^{-1}).

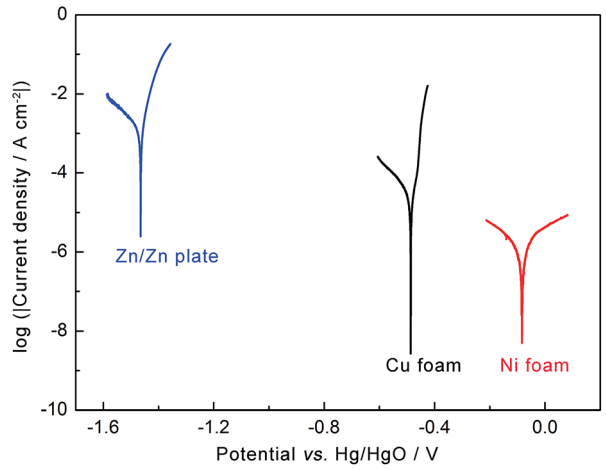

Fig. 1 Tafel plots of different metal substrates (electrolyte: N_2 saturated 7 mol L^{-1} KOH, scan rate: 0.1 mV s^{-1}).

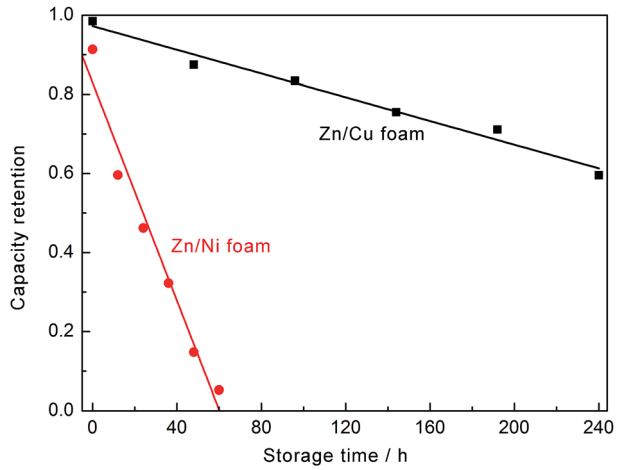

Fig. 3 Capacity retention of Zn/Cu foam and Zn/Ni foam electrodes in zinc/oxygen batteries after different storage time in 7 mol L^{-1} KOH solution (electrolyte: 7 mol L^{-1} KOH, cathode: commercial air electrode, O_2 flow rate: 50 sccm).

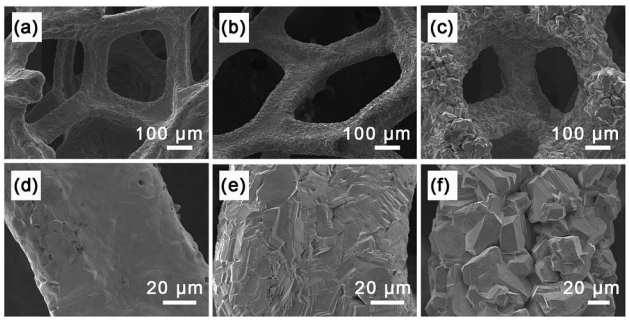

Fig. 4 Morphology of copper foam (a and d), Zn/Cu foam with zinc loading capacity of 20 mA h (b and e) and Zn/Cu foam with zinc loading capacity of 200 mA h (c and f).

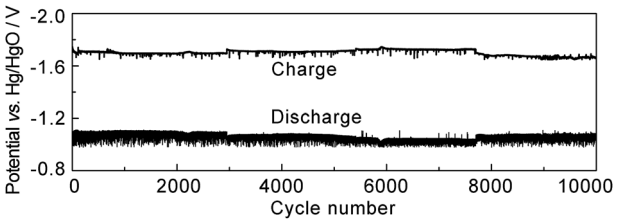

Fig. 6 Potential changes during 10 000 discharge–charge cycles in zinc/zinc quasi-symmetric cell (electrolyte: 8 mol L^{-1} KOH and 0.5 mol L^{-1} ZnO, current density: 250 mA cm^{-2}).

Rate capability and zinc utilization of the Zn/Cu foam electrodes

In order to investigate the rate capability and zinc utilization of the Zn/Cu foam electrodes, primary zinc/oxygen batteries were fabricated, and the *I–V* curves and constant current discharging curves were tested and shown in Fig. 5a and b. The *I–V* curves in Fig. 5a confirm that Zn/Cu foam electrode can bear larger current density for the better electrical conductivity and facilitated mass transport, as a result, a peak power density of 286 mW cm^{-2} is obtained, which increases by 40% in comparison with traditional zinc paste electrode whose peak power density is 205 mW cm^{-2}. Continuous electron transfer passage built by the 3D porous framework of copper foam provides excellent electrical conductivity even after ZnO is formed on the surface of zinc which always hinders electron transfer between zinc particles in traditional zinc paste electrodes. Moreover, diffusion of reactants and products in the aqueous alkaline electrolyte through the interconnected macro-pores encounters less resistance than that in water-containing polymer binders which are widely used in zinc paste electrodes.

The specific capacities of Zn/Cu foam electrodes are calculated to be 799 mA h g^{-1} at 25 and 50 mA cm^{-2}, 796 mA h g^{-1} at 100 mA cm^{-2}, and 754 mA h g^{-1} at 200 mA cm^{-2} from Fig. 5b, which are close to the theoretical specific capacity of 819 mA h g^{-1}. The enhancement of zinc utilization is mainly due to the stable polarization even in the later stage of the discharge by virtue of the uncollapsed copper framework, efficient electron transfer and facilitated mass transport.

Rechargeability of the Zn/Cu foam electrodes

The poor stability of zinc electrodes, due to the shape change and dendrite formation during the discharge–charge period, often lead to poor cycling performance for conventional zinc-based alkaline batteries.[11,20] The persistence of a conductive 3D copper foam substrate, which supports enhanced peak power density and specific capacity in primary zinc/oxygen battery, may also promote the rechargeability of Zn/Cu foam electrode. The control of the dissolution/precipitation process of zinc on copper foam substrate is significantly important to avoid shape change and dendrite formation, and further improves the rechargeability of the zinc-based batteries.

The redox process of zinc in alkaline electrolyte is a multi-phase reaction with Zn^0 being oxidized to Zn^{2+} in the discharge process and Zn^{2+} reduced to Zn^0 in the charge process. The electrode reaction can be described as eqn (1) and (2).

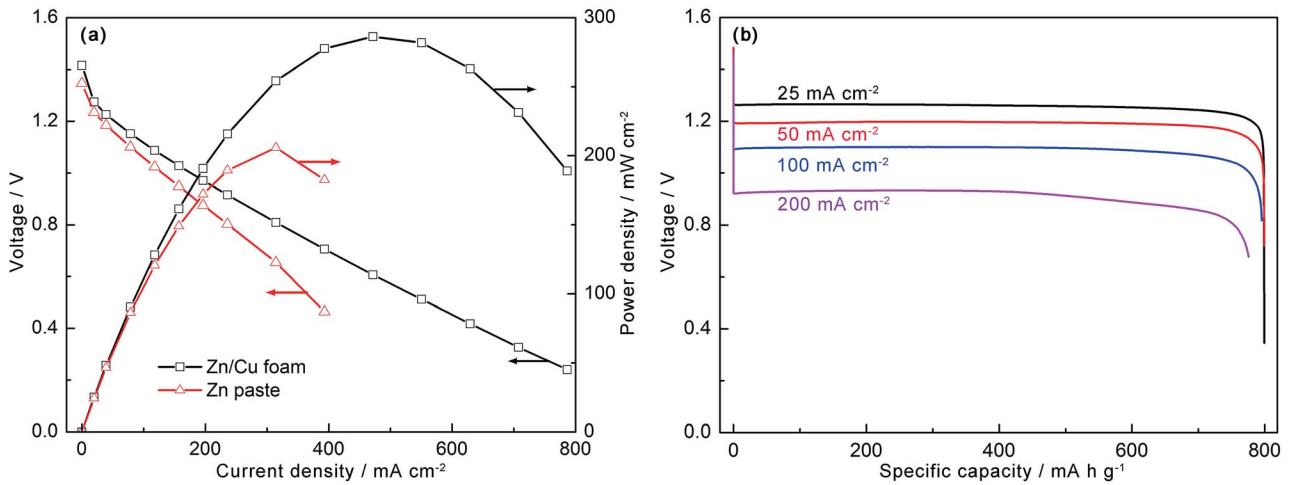

Fig. 5 Electrochemical performance of primary zinc/oxygen batteries (electrolyte: 7 mol L^{-1} KOH, cathode: commercial air electrode, O_2 flow rate: 50 sccm). (a) *I–V* curves with different zinc electrodes; (b) discharge curves at different current densities with Zn/Cu foam electrodes.

Discharge process

$$Zn + 4OH^- = Zn(OH)_4^{2-} + 2e^- \quad (1)$$

Charge process

$$Zn(OH)_4^{2-} + 2e^- = Zn + 4OH^- \quad (2)$$

The electrolyte used in primary zinc/oxygen battery, *i.e.* 7 mol L^{-1} KOH, is not suitable for zinc-based secondary battery due to the large polarization in charge process caused by insufficient concentration of $Zn(OH)_4^{2-}$. Hence, electrolyte containing 8 mol L^{-1} KOH and 0.5 mol L^{-1} ZnO, which increases the amount of $Zn(OH)_4^{2-}$ and maintains the concentration of KOH, is preferred to support smooth dissolution/precipitation process of zinc.

To evaluate the dissolution/precipitation process of zinc at rates one would rarely attempt in a battery, a zinc/zinc quasi-symmetric cell was fabricated by placing Zn/Cu foam electrode between two zinc plate counter electrodes and the discharge–charge cycles were conducted at 250 mA cm^{-2} and 100% DOD. The potential changes of the Zn/Cu foam electrode in 10 000 discharge–charge cycles are shown in Fig. 6. With the continuous structure, electrical conductivity of the Zn/Cu foam electrode maintains even after all the active materials change to ZnO or $Zn(OH)_4^{2-}$, which can hardly be realized in traditional zinc paste electrode where zinc products always block electron

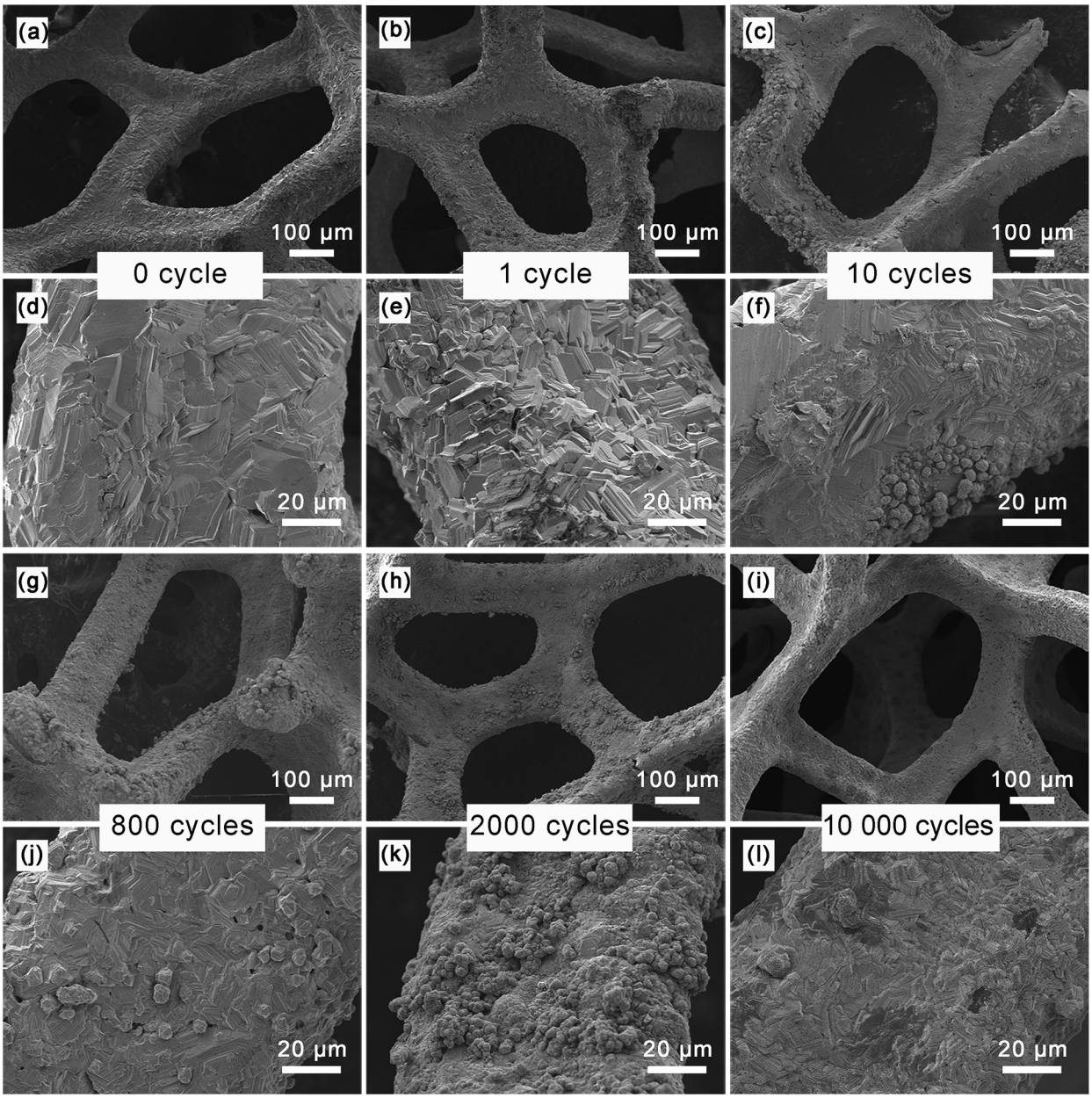

Fig. 7 Morphology changes of Zn/Cu foam electrodes after different discharge–charge cycles in zinc/zinc quasi-symmetric cell.

transfer by covering and separating the active materials. It can be seen from Fig. 6 that overpotentials of both discharge and charge processes are around 0.3–0.35 V *vs.* open circuit potential of Zn/Cu foam electrode and change slightly in 10 000 discharge–charge cycles which means conductivity and 3D continuous structure of Zn/Cu foam electrode keep invariant in these cycles. Fig. 7 shows the morphology of Zn/Cu foam electrodes at different cycling times. After the first discharge–charge cycle, zinc becomes rougher (Fig. 7b and e) for that pulse electro-deposition in Zn/Cu foam preparation is replaced by constant current charging. Aggregation occurs after 10 discharge–charge cycles and particles round 1–5 μm are found in some part of the Zn/Cu foam structure (Fig. 7c and f). When discharge–charge cycles increase to 800 times (Fig. 7g and j), more particles are aggregated and about 30% of the surface are covered with zinc particles after 2000 discharge–charge cycles (Fig. 7h and k). However, at the end of 10 000 discharge–charge cycles, both aggregation of zinc particles and epitaxial layers of zinc crystal become inconspicuous (Fig. 7i and l) which may result from the self-corrosion of zinc in alkaline electrolyte. Discharge–charge cycles of Zn/Cu foam electrode were performed at conditions prone to form dendrite: fast charge process, large discharge depth, long cycling times and without dendrite-suppressing additives. Only tiny aggregation and leaching appear, while no dendrite is observed during the cyclings, which confirms an unprecedented stability of Zn/Cu foam electrode.

Performance of the secondary Zn/Ni battery

Secondary Zn/Ni batteries were developed for military applications and electric vehicles from 1960s for their high specific energy, however, limited cycling lifetime related to the zinc electrode hindered the commercialization of Zn/Ni batteries.[20,21] A prototype Zn/Ni battery comprising a Zn/Cu foam electrode and two commercially available sintered nickel electrodes was assembled following on the successful cycling Zn/Cu foam electrode in a quasi-symmetric cell.

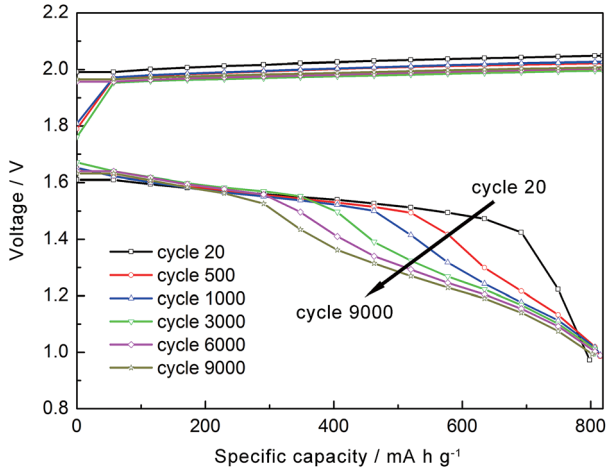

Fig. 8 Typical discharge–charge curves of secondary Zn/Ni battery using Zn/Cu foam negative electrode and commercial sintered nickel positive electrode (current density: 100 mA cm^{-2}).

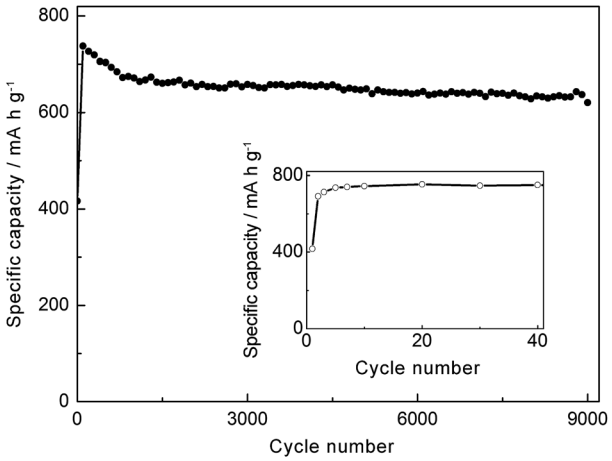

Fig. 9 Specific capacity of Zn/Cu foam electrode in secondary Zn/Ni battery with a cut-off voltage of 1.2 V.

To balance the test time and battery polarization, discharge–charge current densities of 100 mA cm^{-2}, which were still severer than some researches,[11,13] were chosen for the prototype secondary Zn/Ni battery. The typical discharge–charge curves are displayed in Fig. 8. It can be seen that specific capacities with a cut-off voltage of 1.0 V are close to the theoretical specific capacity which confirms that zinc is eliminated in each discharge process and thus the accumulation of active materials is avoided. Battery voltage decrease in the later stage of discharge processes with the increase in cycling times indicates performance degradation of the prototype secondary Zn/Ni battery which can be confirmed by the specific capacity changes with the cut-off voltage of 1.2 V shown in Fig. 9. Specific capacity of zinc electrode increases to 753.8 mA h g^{-1} at the 20th discharge process after the initial activation and gradually decreases to 620 mA h g^{-1} at the 9000th cycle (Table S1 and S2†). Capacity fade mainly occurs in the early 1500 cycles where 12% capacity is decreased, while capacity drop is reduced to 6% in the following 7500 cycles. The excellent stability and specific

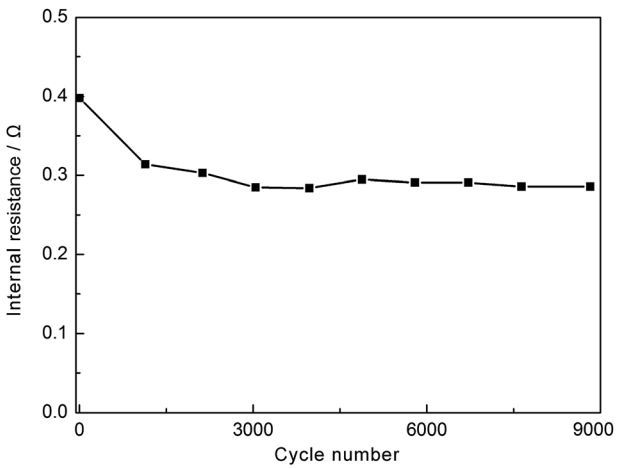

Fig. 10 Internal resistance changes of secondary Zn/Ni battery during 9000 discharge–charge cycles.

capacity of Zn/Cu foam electrode benefiting from the stable 3D structure and conductivity of zinc electrode with a copper foam substrate are consistent with the results from the zinc/zinc quasi-symmetric cell. Internal resistance of the secondary Zn/Ni battery obtained from electrochemical impedance spectroscopy is *ca.* 0.4 Ω before cycling and reduces to *ca.* 0.3 Ω and keeps almost unchanged during 9000 discharge–charge cycles (Fig. 10 and S7†). This result confirms the maintenance of porous structure and conductivity of the Zn/Cu foam electrode.

Conclusions

In this work, Zn/Cu foam electrodes for zinc-based alkaline batteries were prepared by pulse electro-depositing zinc on 3D continuous copper foam, and tested in primary zinc/oxygen batteries, zinc/zinc quasi-symmetric cells and a secondary Zn/Ni battery. Benefiting from the interconnected metal skeleton which provides facilitated electron transfer and mass transport, as well as the porous structure which provides large electrochemically active surface area for uniform distribution of active materials, zinc/oxygen battery using Zn/Cu foam electrode presents a peak power density of as high as 286 mW cm^{-2} and a large specific capacity of 754 mA h g^{-1} at 200 mA cm^{-2} discharge. Resulting from the large hydrogen evolution overpotential on copper substrate which suppresses self-corrosion of zinc efficiently and the stable copper framework throughout the discharge–charge period which avoids electrode collapse, Zn/Cu foam electrode can bear 10 000 dendrite-free discharge–charge cycles with 100% DOD of zinc. A prototype secondary Zn/Ni battery retains the specific capacity of 620 mA h g^{-1} for the Zn/Cu foam electrode after 9000 discharge–charge cycles at 100 mA cm^{-2}. These results suggest that Zn/Cu foam electrode possesses superior cycling stability, high rate capability and outstanding metal utilization, which is a promising candidate for zinc-based alkaline batteries.

Acknowledgements

This work is financially supported by the National Basic Research Program of China (2012CB215500) and the Youth Innovation Promotion Association of CAS (2012153).

References

1 A. Sternberg and A. Bardow, *Energy Environ. Sci.*, 2015, **8**, 389–400.
2 K. Nemeth and G. Srajer, *RSC Adv.*, 2014, **4**, 1879–1885.
3 H. Ma and B. Wang, *RSC Adv.*, 2014, **4**, 46084–46092.
4 M. Gong, Y. Li, H. Zhang, B. Zhang, W. Zhou, J. Feng, H. Wang, Y. Liang, Z. Fan, J. Liu and H. Dai, *Energy Environ. Sci.*, 2014, **7**, 2025–2032.
5 R. P. Hamlen and T. B. Atwater, in *Handbook of Batteries*, ed. D. Linden and T. B. Reddy, McGraw-Hill, New York, 3rd edn, 2002, pp. 38.1–38.53.
6 D. Geng, N.-N. Ding, T. S. A. Hor, S. W. Chien, Z. Liu and Y. Zong, *RSC Adv.*, 2015, **5**, 7280–7284.
7 Y. Cheng, Q. Lai, X. Li, X. Xi, Q. Zheng, C. Ding and H. Zhang, *Electrochim. Acta*, 2014, **145**, 109–115.
8 M. N. Masri and A. A. Mohamad, *J. Electrochem. Soc.*, 2013, **160**, A715–A721.
9 X. G. Zhang, *J. Power Sources*, 2006, **163**, 591–597.
10 C. Tang, D. Zhou, S. Fang and L. Yang, *J. Electrochem. Soc.*, 2012, **159**, A1796–A1800.
11 J. F. Parker, C. N. Chervin, E. S. Nelson, D. R. Rolison and J. W. Long, *Energy Environ. Sci.*, 2014, **7**, 1117–1124.
12 J. F. Parker, E. S. Nelson, M. D. Wattendorf, C. N. Chervin, J. W. Long and D. R. Rolison, *ACS Appl. Mater. Interfaces*, 2014, **6**, 19471–19476.
13 Y. Cheng, H. Zhang, Q. Lai, X. Li, D. Shi and L. Zhang, *J. Power Sources*, 2013, **241**, 196–202.
14 Y. F. Yuan, J. P. Tu, H. M. Wu, Y. Z. Yang, D. Q. Shi and X. B. Zhao, *Electrochim. Acta*, 2006, **51**, 3632–3636.
15 Y. F. Yuan, L. Q. Yu, H. M. Wu, J. L. Yang, Y. B. Chen, S. Y. Guo and J. P. Tu, *Electrochim. Acta*, 2011, **56**, 4378–4383.
16 Y. Wen, T. Wang, J. Cheng, J. Pan, G. Cao and Y. Yang, *Electrochim. Acta*, 2012, **59**, 64–68.
17 Y. Ito, M. Nyce, R. Plivelich, M. Klein, D. Steingart and S. Banerjee, *J. Power Sources*, 2011, **196**, 2340–2345.
18 B. Yang and Z. Yang, *RSC Adv.*, 2013, **3**, 12589–12592.
19 S. H. Lee, C. W. Yi and K. Kim, *J. Phys. Chem. C*, 2011, **115**, 2572–2577.
20 R. Wang and Z. Yang, *RSC Adv.*, 2013, **3**, 19924–19928.
21 D. Coates and A. Charkey, in *Handbook of Batteries*, ed. D. Linden and T. B. Reddy, McGraw-Hill, New York, 3rd edn, 2002, pp. 31.1–31.37.